ORNL/TM-2023/3118
M3LW-23OR0402027

Microstructure and In-Service Degradation of Baffle-Former Bolts – In-Core Components of Light-Water Reactors

M. Gussev
T. Lach
X. Chen

Approved for public release.

September 2023

OAK RIDGE National Laboratory

ORNL IS MANAGED BY UT-BATTELLE LLC FOR THE US DEPARTMENT OF ENERGY

ORNL/TM-2023/3118
M3LW-23OR0402027

Nuclear Energy and Fuel Cycle Division
Materials Science and Technology Division

MICROSTRUCTURE AND IN-SERVICE DEGRADATION OF BAFFLE-FORMER BOLTS – IN-CORE COMPONENTS OF LIGHT-WATER REACTORS

M. Gussev
T. Lach
X. Chen

September 2023

Prepared under the direction of the
U.S. Department of Energy
Office of Nuclear Energy
Light Water Reactor Sustainability Program
Materials Research Pathway

Prepared by
OAK RIDGE NATIONAL LABORATORY
Oak Ridge, TN 37831
managed by
UT-BATTELLE, LLC
for the
U.S. DEPARTMENT OF ENERGY
under contract DE-AC05-00OR22725

CONTENTS

LIST OF FIGURES

LIST OF TABLES

ABBREVIATIONS

AGG	abnormal grain growth
AISI	American Iron and Steel Institute
APT	atom probe tomography
BFB	baffle-former bolt
BSE	backscatter electrons
DOE	US Department of Energy
dpa	displacement per atom
EBSD	electron backscatter diffraction
EDS	energy-dispersive X-ray spectroscopy
fcc	face-centered cubic
FIB	focused ion beam
GB	grain boundary
GROD	grain reference orientation deviation
IMET	Irradiated Materials Examination and Testing Facility
IPF	inverse pole figure
IQ	image quality
KAM	kernel average misorientation
LAB	in-grain low-angle boundary
LAMDA	Low Activation Materials Development and Analysis Laboratory
LWR	light water reactor
ORNL	Oak Ridge National Laboratory
NPP	nuclear power plant
PWR	pressurized water reactor
RHAB	random high-angle boundary
ROI	region of interest
SEM	scanning electron microscopy
YS	yield stress

ACKNOWLEDGMENTS

This research was supported by the US Department of Energy, Office of Nuclear Energy, Light Water Reactor Sustainability Program, Materials Research Pathway. Valuable help and support from the staff at the Oak Ridge National Laboratory (ORNL) Low Activation Materials Development and Analysis Laboratory (LAMDA) (T. Dixon, K. Everett, P. Tedder, S. Curlin) and Radiation Control Technician Office are gratefully acknowledged. The authors thank Dr. C. McKinney (ORNL) for reviewing the report and R. Raney (ORNL) for helping with document preparation.

EXECUTIVE SUMMARY

This report presents a microstructure evaluation of the baffle former bolt, a commercial pressurized water reactor component. Using scanning electron microscopy (SEM), energy-dispersive x-ray spectroscopy (EDS), and electron backscatter diffraction (EBSD), analysis of the material was identified as American Iron and Steel Institute (AISI) 316 steel with an annealed austenite microstructure. Findings include abnormal grain growth in a fraction of the grains and the absence of retained ferrite. Notable observations include pre- and post-irradiation deformation overlap, including defect-free channel formation as an active deformation mechanism in the near-surface layer of baffle-former bolts (BFBs).

Specimen surfaces that are exposed to high-temperature, high-pressure water exhibited signs of in-service corrosion degradation. EBSD and EDS analyses highlighted intergranular corrosion, possible grain boundary oxidation at depths of less than 3 μm, and unexpectedly, short cracks filled with Cr-rich oxides measuring approximately 5–6 μm.

The presence of defect-free channels seen in EBSD data suggests that there were episodes of high mechanical stress during service. The specimens provide a potentially unique insight into the in-service degradation of nuclear power plant (NPP) components, strain localization, and crack initiation processes. An intact corrosion layer reveals a complex component's in-service history. Further research is underway in the form of a detailed analysis.

1. INTRODUCTION

Baffle-former bolts (BFBs) are important pressurized water reactor (PWR) parts. While in service in the reactor core during plant operation, BFBs and other components can incur radiation-induced degradation aggravated by the corrosive environment. Material degradation may reduce the load-carrying capacity and eventually lead to cracking. BFB degradation and cracking has been a concern for the nuclear industry since the 1980s. Degraded BFBs were first observed in the United States in 1999.

To study the long-term operational performance and reliability of BFBs, the US Department of Energy (DOE) Oak Ridge National Laboratory (ORNL), under the DOE Light Water Reactor Sustainability Program's Materials Research Pathway, attempted to harvest two high-fluence BFBs from a commercial Westinghouse two-loop downflow-type PWR. These BFBs had the highest fluence among bolts withdrawn from service in 2011 and did not exhibit any indications of cracking according to routine ultrasonic and visual inspection. The goal was to study the microstructural, mechanical, and corrosion-related properties of the BFBs and estimate the performance of the same components remaining in service.

Two high-fluence BFBs were successfully harvested from a Westinghouse PWR in 2016 and received at the Westinghouse facility for specimen fabrication. The manufactured specimens were delivered to ORNL, where fracture mechanics testing [1,2], advanced microstructure analysis [3,4], and pilot in situ mechanical tests [5] were performed.

Additional specimens were transferred to the Low Activation Materials Development and Analysis Laboratory (LAMDA) at ORNL during FY2023 to perform microstructure analysis. This report documents the most recent results, including pre- and post-service deformation, localized strain (defect-free channel formation suggesting episodes of component loading), and in–service–induced corrosion damage. Degraded grain boundaries and several short corrosion cracks were observed and characterized using scanning electron microscopy (SEM), electron backscatter diffraction (EBSD), and energy dispersive X-ray spectroscopy (EDS). The results presented here underline the importance of studying in-reactor material degradation in commercial PWRs.

2. MATERIALS

2.1 HARVESTED BAFFLE-FORMER BOLTS

Table 1 provides information on the range of fluences and estimated displacement damage along the lengths of the two bolts [1,4]. The displacement damage values for the two bolts range from 15 to 41 dpa, assuming a fluence-to-displacements per atom (dpa) conversion value of 6.7×10^{20} n/cm^2, $E > 1$ MeV/dpa [6]. Additional information (irradiation temperature profile, flux) is not available at the time of report preparation.

Table 1. Fluence and estimated displacement damage distributions for two retrieved BFBs

Bolt ID	Fluence (10^{22} n/cm^2, E > 1 MeV) and estimated damage dose in dpa for different portions of BFBs					
	Head		Mid-shank		Mid-thread	
	Fluence	Dose	Fluence	Dose	Fluence	Dose
4412	2.78	41	2.27	34	1.46	22
4416	1.91	29	1.56	23	1.00	15

The specimen machining scheme and specimen IDs are shown in Figure 1. For each BFB, four bend-bar specimens and seven thin-slice specimens were machined. The bend-bar specimens were used in the fracture toughness and fatigue crack growth rate studies [2]. In contrast, the thin-slice specimens were designated for microstructural analyses [3] and advanced mechanical testing [5].

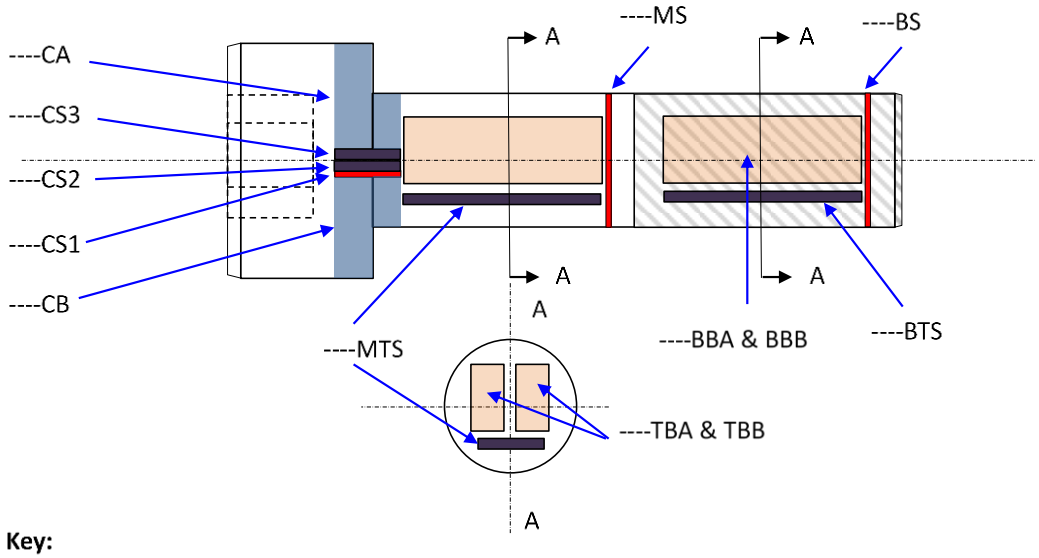

Key:
----: bolt number, **CS**: collar slice, **CA & CB**: remaining collar materials, **MS**: middle slice, **BS**: bottom slice, **MTS**: middle thick slice, **BTS**: bottom thick slice, **TBA & TBB**: top bend bar, **BBA & BBB**: bottom bend bar

Figure 1. Bolt cutting scheme and IDs for cut objects [1]. References [1,2,4] provide more detail.

In the present work, the 4412-CS1 specimen (cross-section slice of the bolt #4412 head portion, Figure 2a, b) was also cut into several smaller pieces, as seen in Figure 2c, to reduce activity level. The 4412-CS-1-1 and 4412-CS-1-2 specimens were transferred to the LAMDA facility for additional preparation and microstructural analysis.

For EBSD analysis purposes, electropolishing is usually a better option, but it removes excess material at the specimen's edges, making analysis of this area impossible. Therefore, electropolishing was rejected in this particular case, so the specimens were mounted in epoxy, mechanically ground, and polished using standard metallography procedures. Colloidal silica polishing was the last preparation step. Upon preparation, the specimens were extracted from epoxy (the epoxy was dissolved using appropriate reagents), cleaned from epoxy residuals using an appropriate solvent, and stored in a membrane box. During preparation, thickness removal was intentionally limited to preserve valuable objects and to ensure that more thickness would be available if additional polishing was needed.

Microstructure analysis was performed using TESCAN MIRA3 SEM. The SEM is equipped with an Oxford Symmetry EBSD detector and an Oxford Ultim Max 170 EDS detector.

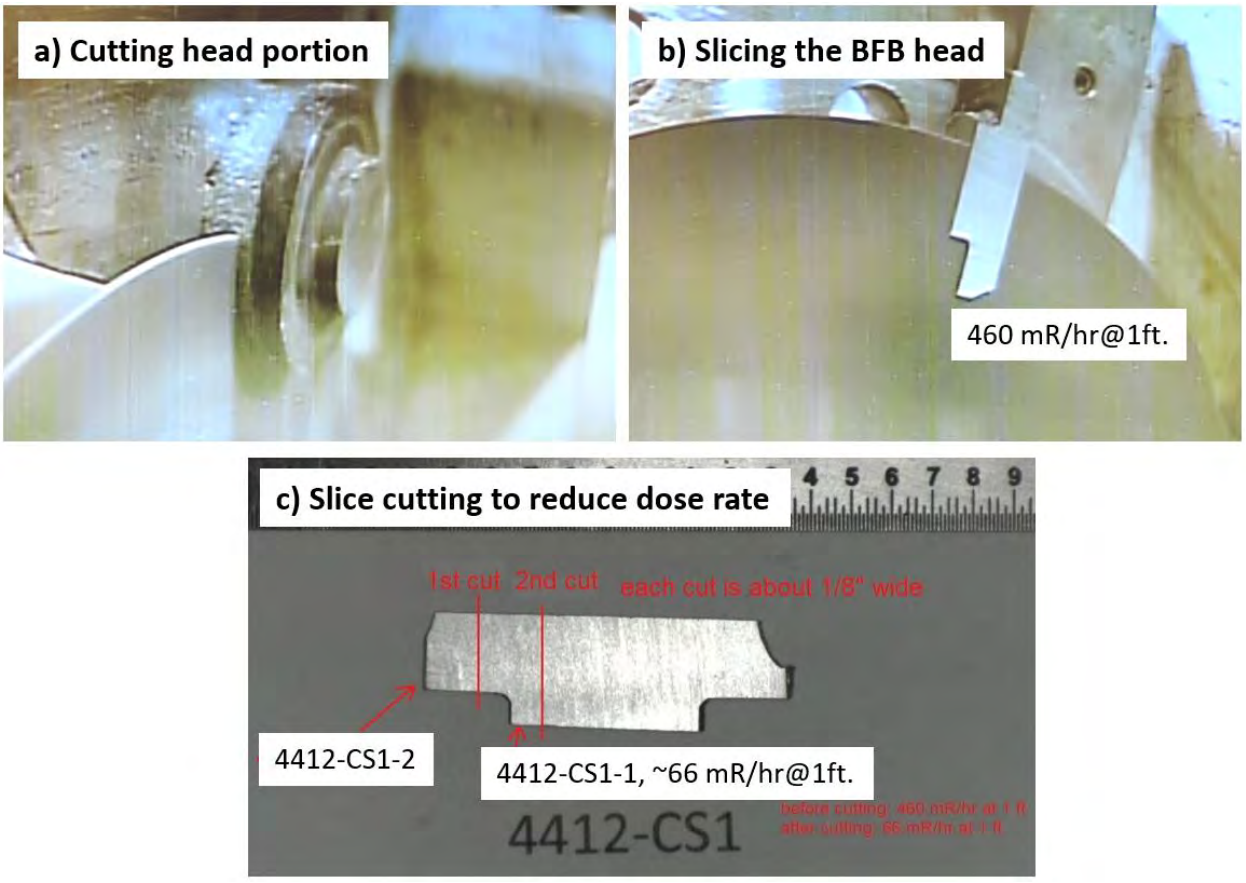

Figure 2. Images taken at different steps of BFB cutting and slicing. Note that the dose rate value for the 4412-CS-1-1 specimen was close to LAMDA limits (100 mR/h@1ft).

3. EXPERIMENTAL ACTIVITIES

3.1 BFB BASIC MICROSTRUCTURE

Figure 3 shows the general view of the 4412-CS-1-1 specimen; an insert in the right corner demonstrates specimen origin and orientation concerning the baffle bolt axis. It can be observed that most of the as-prepared specimen surface had a high-quality EBSD-suitable surface. Approximately ⅓ of the surface (shown in the bottom portion of Figure 4) still had an as-cut surface with low-speed saw marks. EBSD scans were performed at several locations (Figure 3) to investigate microstructure conditions and to target future focused ion beam (FIB) liftouts.

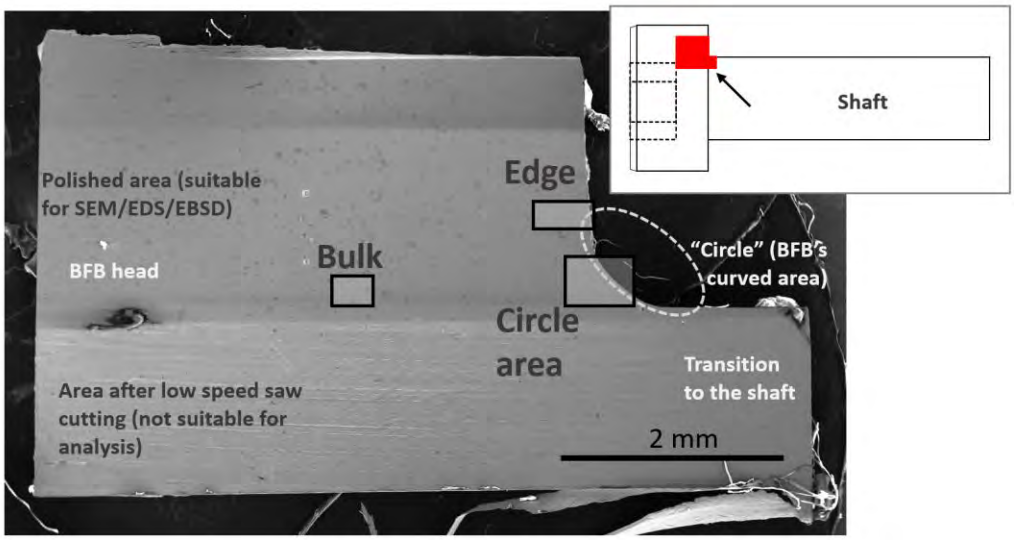

Figure 3. General view of the 4412-CS-1-1 specimen from the BFB head portion.
Bulk, *Edge*, and *Circle area* labels show the locations of EBSD scans discussed herein. The inset at the right top shows the geometry and orientation of the specimen within the source bolt.

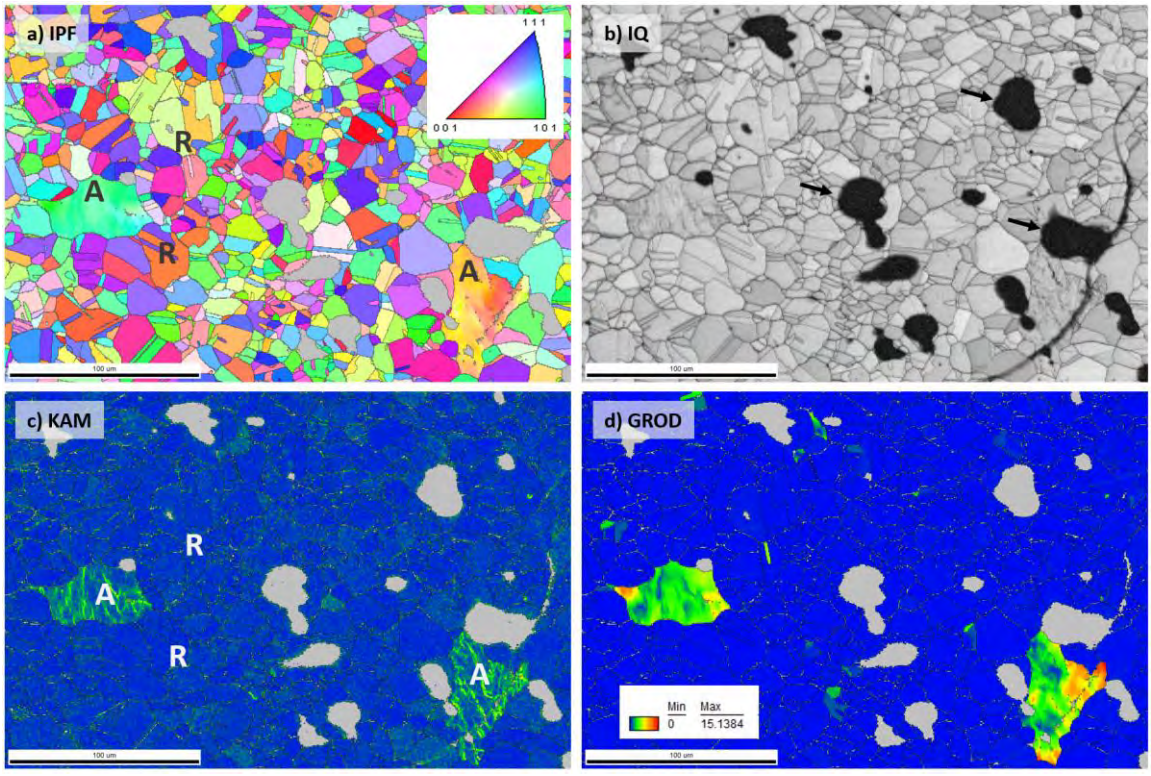

Figure 4. Microstructure of the BFB head (bulk area, ~2 mm from the edge; see Figure 3 for specimen location and orientation). A dominating recrystallized microstructure (several typical recrystallized grains are marked with an *R* label) can be observed, with a few grains with high in-grain misorientation levels (marked as *A* for *abnormal*). Carbon contamination spots are marked with arrows in the image quality (IQ) map. The inverse pole figure (IPF) color key is the same for all images in the document. All IPFs are colored in the horizontal direction.

Figure 4 shows the typical microstructure for the BFB material in the 4412-CS-1-1 specimen. Typical equiaxial austenite grains dominate in the structure; such grains (some are marked as *R*, indicating *recrystallized*; see an enlarged grain view in Figure 5a) have no in-grain color variations, indicating minor misorientation gradients. No or negligible in-grain orientation gradients are present for such grains in kernel average misorientation (KAM) and grain reference orientation deviation (GROD) maps. No retained ferrite was observed in the structure.

Some grains show pronounced in-grain misorientation variations (see IPF map; grains are marked as *A*, indicating *abnormal*, an example is given in Figure 5b). The KAM map for such grains clearly shows in-grain low-angle boundaries (LABs) most likely from dislocation. The GROD maps reveal in-grain misorientation levels up to 15°, suggesting elevated dislocation densities. A population of recrystallized grain fully surrounds such abnormal grains, ruling out the possibility that cold work (occasional or intentional deformation) was a possible source of the elevated in-grain misorientation levels. KAM distribution inside such abnormal grains is also not typical for cold or warm deformation in reference (non-irradiated) steel or strain localization processes in irradiated steel.

These abnormal grains are much larger than the surrounding fully recrystallized grains. The specific shape of grain boundaries (arcs or semicircles) suggests that these grains may be a result of abnormal grain growth (AGG) [7] (sometimes termed also as “anomalous grain growth”). The AGG usually occurs if the material has experienced some threshold deformation level and remained at higher temperatures longer than necessary to complete recrystallization. The presence of some texture components may be a factor influencing AGG. Although there is limited literature evidence, elevated levels of in-grain misorientation may be connected to the AGG phenomenon, such as through the consumption of neighboring grains. An additional focused study may be necessary to understand these aspects.

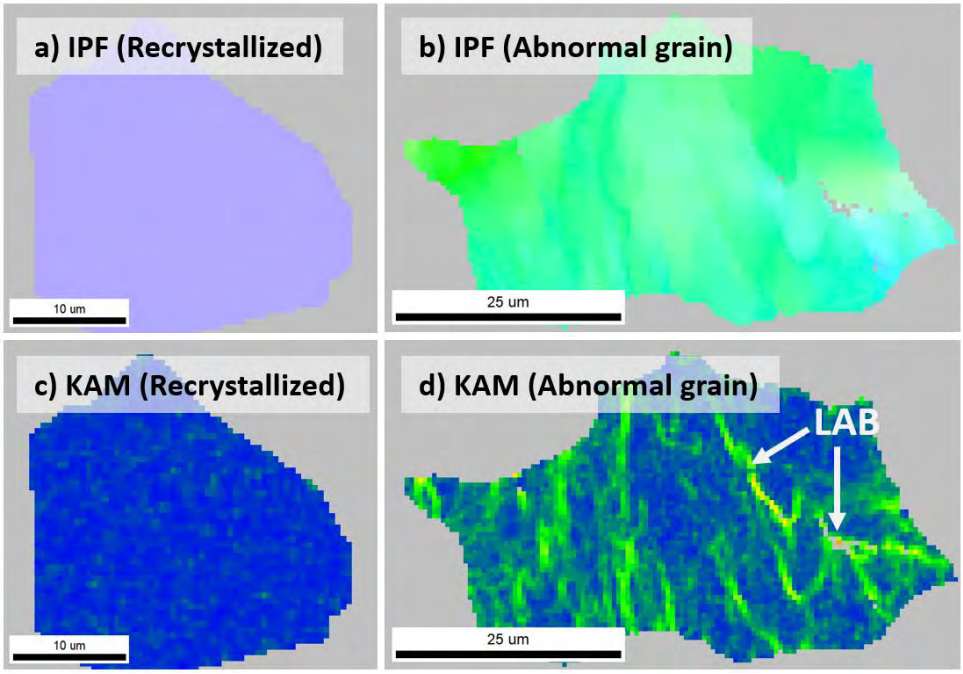

Figure 5. Typical recrystallized (a) and abnormal (b) grains for BFB bulk microstructure shown in Figure 4.(c, d) KAM maps showing in-grain misorientation. LAB: in-grain low-angle boundaries.

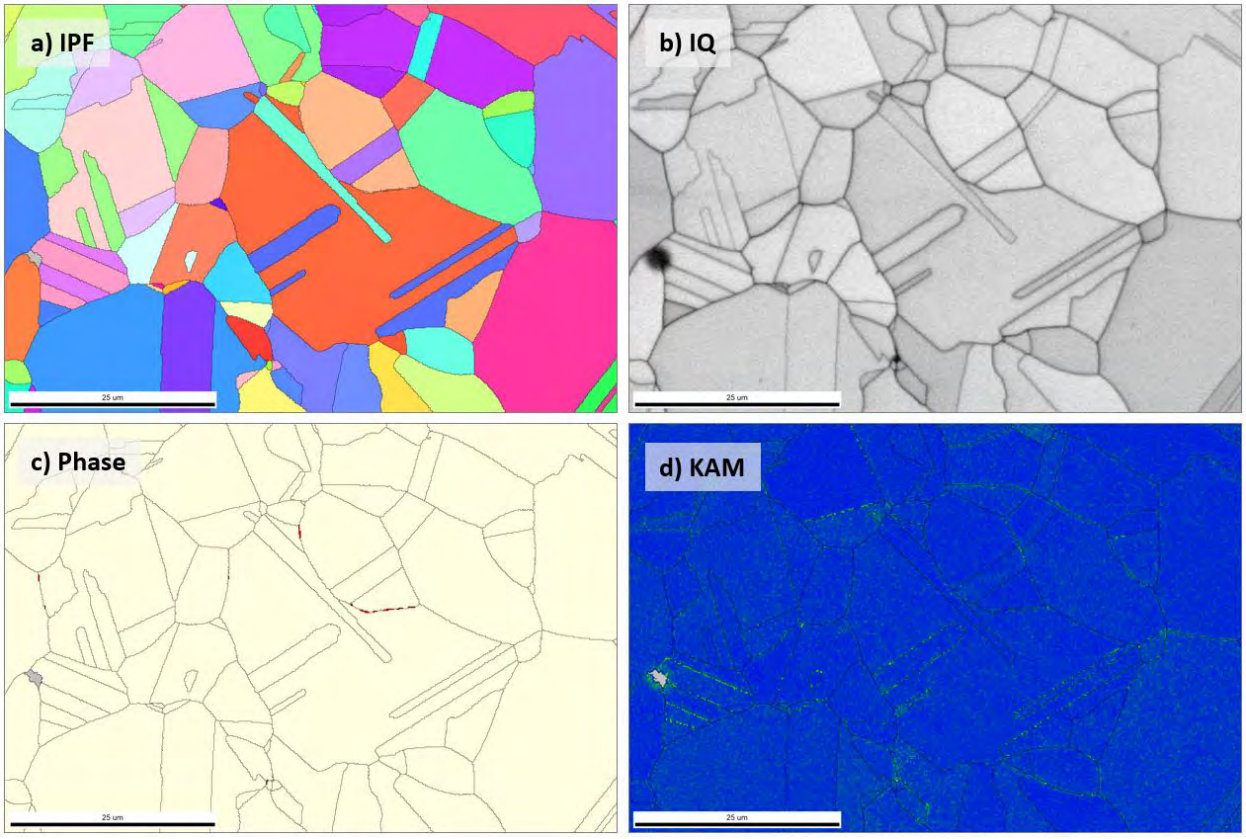

Figure 6. Subarea of bulk EBSD scan seen in Figure 4, rescanned with 125 nm step. An annealed austenite structure with equi-axial grains can be seen. Note the relatively small average grain size of ~20 µm.

Figure 6 shows the subarea of the bulk EBSD scan. If abnormal grains are excluded, then the remainder of the microstructure consists of typical annealed austenite with multiple annealing twins. No obvious signs of pre- or post-irradiation deformation (e.g., lattice orientation gradients along grain boundaries, fine slip lines, or coarse defect-free channels) are present in the BFB interior.

The microstructure conditions should be reexamined for other locations, such as slices from the shaft. The manufacturing and thermal history may not correspond exactly to the 4412-CS-1-1 specimen location. For instance, 4416-MS specimens (middle of the bolt shaft) clearly showed pre-irradiation cold or warm deformation [5].

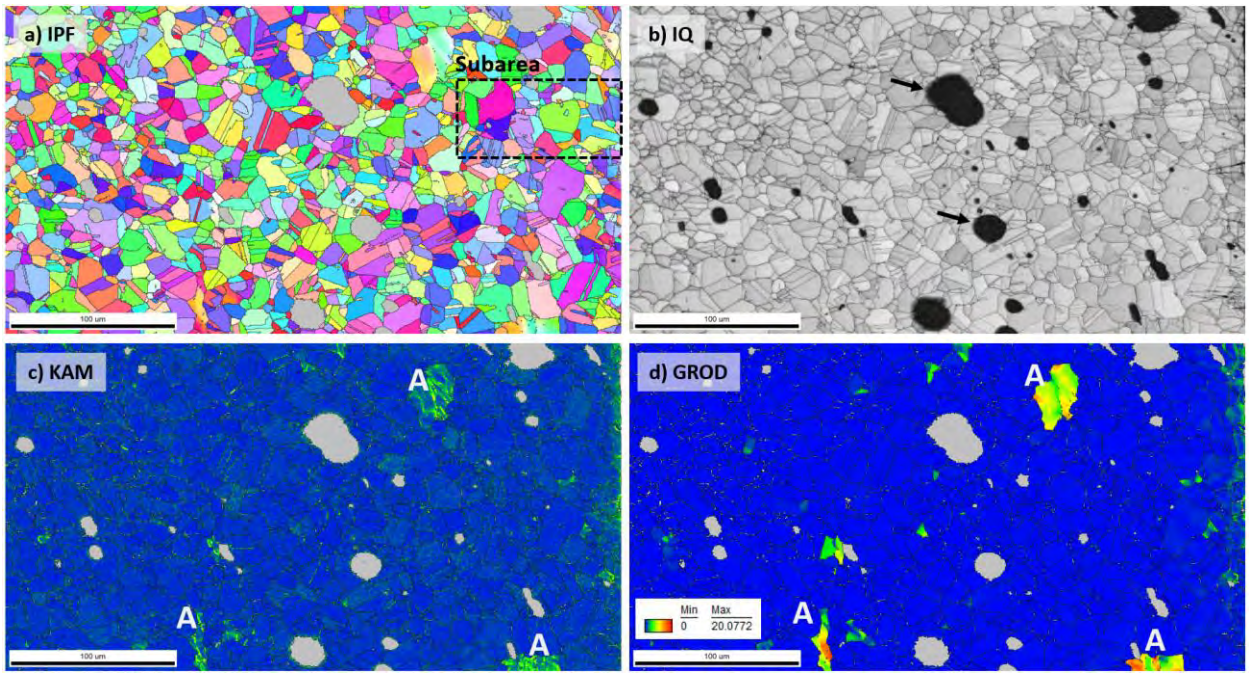

Figure 7. Microstructure of the BFB head (edge area; see Figure 3 for specimen location and orientation). A dominating recrystallized microstructure with a few abnormal grains (marked as *A*) can be seen. Carbon contamination spots are indicated with arrows in the IQ map. The subarea was rescanned using a smaller EBSD step, as seen in Figure 8.

Figure 7 shows the microstructure of the BFB edge area; this location is close to the edge. Analysis of the EBSD maps (especially KAM and GROD) shows mostly annealed austenite with a few abnormal grains. The general appearance of the edge area microstructure is very close to the bulk area (Figure 6). The only significant difference is the appearance of the area on the right, which contains obvious signs of plastic deformation. The layer with increased KAM and GROD values has a ~15–20 μm thickness. This may suggest that the thin near-surface layer was subjected to local loading and deformation.

A small subarea was rescanned with a reduced EBSD step size of 125 nm, as shown in Figure 8. The presence of a thin ~15 μm deformed layer is obvious. The misorientation pattern (smooth changes in GROD, absence of hot spots typical for irradiated austenitic steel [8]) indicates that this near-surface deformation occurred before irradiation. Additionally, the deformation could occur at small damage doses of less than ~1 dpa, which are insufficient to stimulate defect-free channel formation.

Of special interest is the IQ map shown in Figure 8b, which illustrates the quality of the EBSD patterns. Although IQ (Kikuchi pattern image quality) is a qualitative parameter (better/worse), it decreases as defect density increases (e.g., dislocation density increase near the dislocation pile-up) and near grain boundaries, inclusions, phase boundaries, and so on. The map in Figure 8 clearly shows preparation-induced scratches intersecting the whole view field. The scratches are formed by hard particles rolling along the specimen's surface. Commercial alloys often have metallurgical or second-phase inclusions that fall off during specimen preparation. Hard inclusions easily generate scratches, and because inclusions are supplied by material volume, scratching may be difficult to avoid entirely. Because a scratch is a subsurface plastic strain, it will overlap with strain from other sources. As a rule, scratches form straight lines that intersect grain boundaries without changing direction. Except in coincidental cases, scratches do not follow slip plane traces (e.g., (111)-planes in face-centered cubic (fcc) materials).

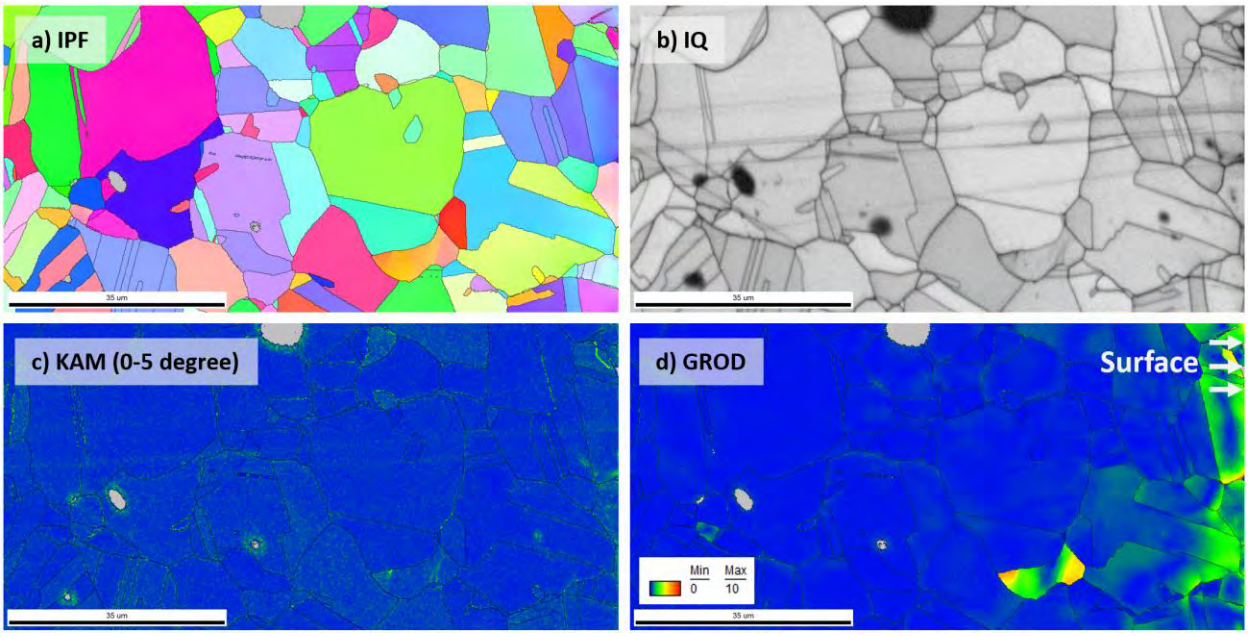

Figure 8. A magnified view of the subarea shown in Figure 7. The BFB edge (surface) is shown on the right in each image.

Figure 9 shows the microstructure of the *circle area* shown in Figure 3; the same pattern of dominating annealed grains mixed with abnormal grains can be seen. The abnormal grains are more abundant here, forming specific groups or lines. Such groups are elongated in the direction parallel to the edge, likely reflecting some preexisting texture or deformation structures related to BFB manufacturing. Also, there is a thin, slightly deformed layer along the edge with a thickness estimated at 10–15 µm.

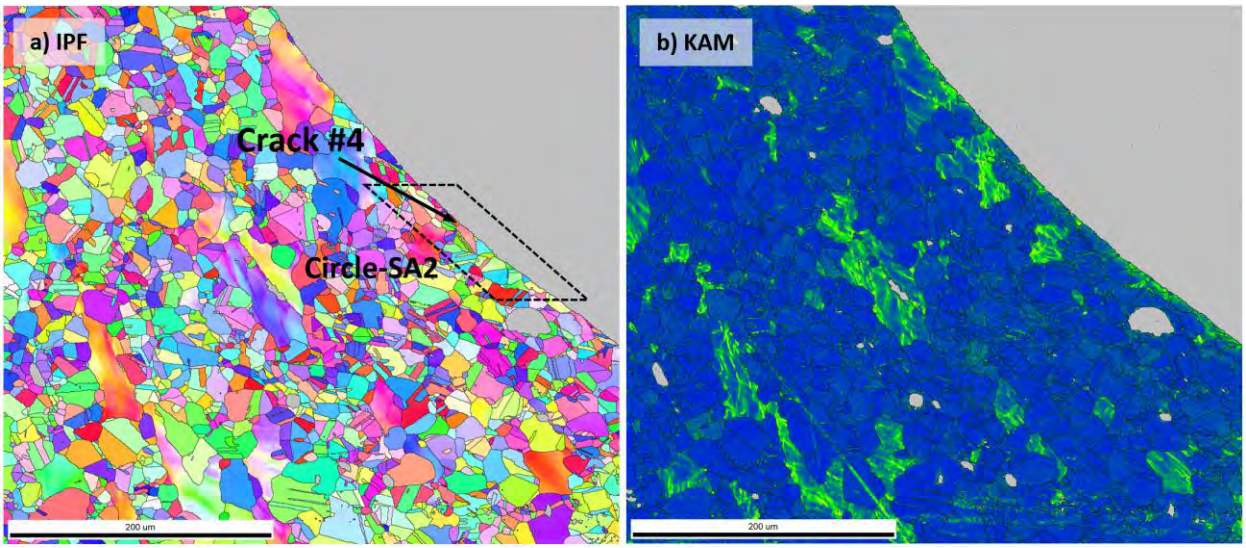

Figure 9. The microstructure of the *circle area* shown in Figure 3.

3.2 CORROSION DAMAGE AT THE HEAD-SHANK TRANSITION

The detailed survey of the 4412-CS-1-1 specimen brought up the unexpected result depicted in Figure 10. The SEM images along the edge showed features resembling short corrosion cracks. Based on the grain contrast shown in the SEM / backscatter electron (BSE)-images, all features were related to grain boundaries. Evidence of mechanical damage was minimal, thus ruling out indents or mechanical contact with a sharp object as a cause for damage. The features are believed to be caused by corrosion and were most likely formed in-service during irradiation.

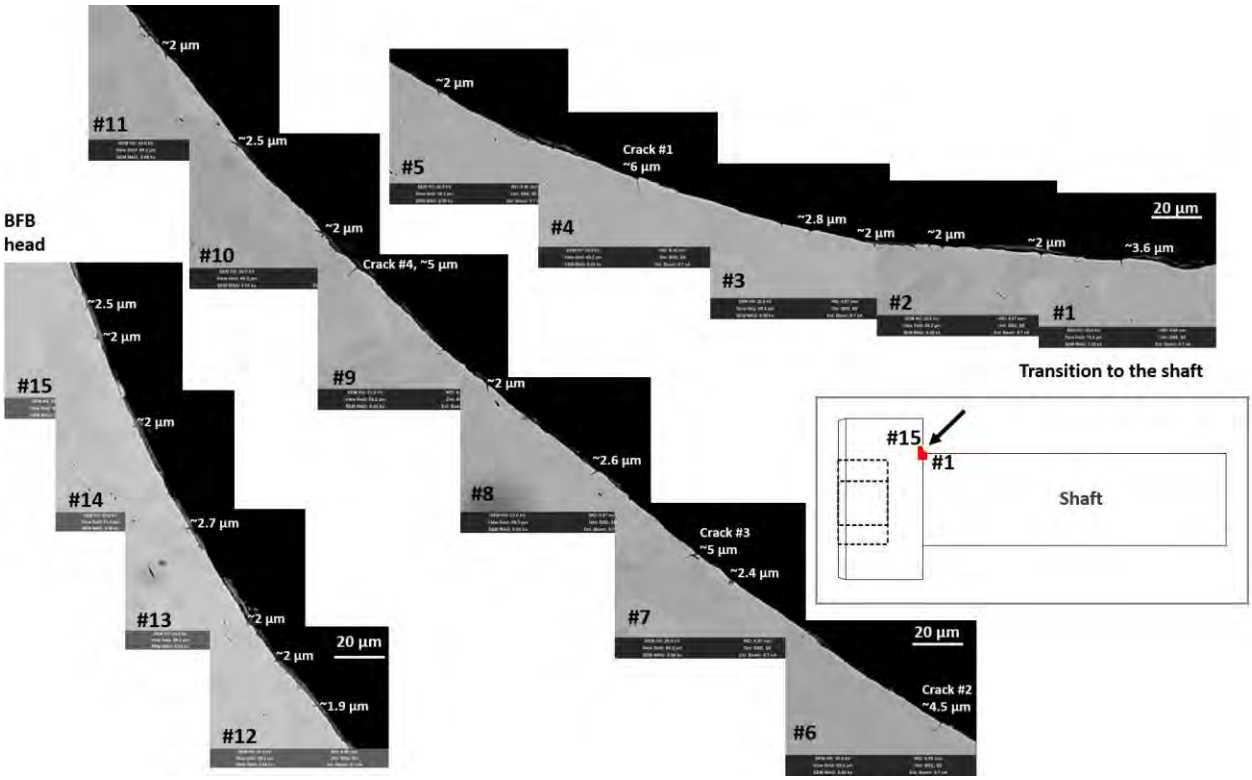

Figure 10. SEM-image collage (BSE-detector, zero-degree SEM stage tilt) showing corrosion damage distribution and depth. Image #1 (right) was taken close to the BFB shaft, and image #15 was recorded close to the BFB head.

The depths of most features from the surface varied between 2 and 3 µm, but a few exceeded ~4 µm. Morphology variations between these features and the histogram plot in Figure 11 suggest two types of damage: shallow pit-like objects or degraded grain boundaries 2–3 µm in depth, as well as deeper 4 µm+ features appearing as short cracks. These deep crack-like formations were in the middle of a curved area, whereas the circled area's beginning and end had only shallow degraded grain boundaries.

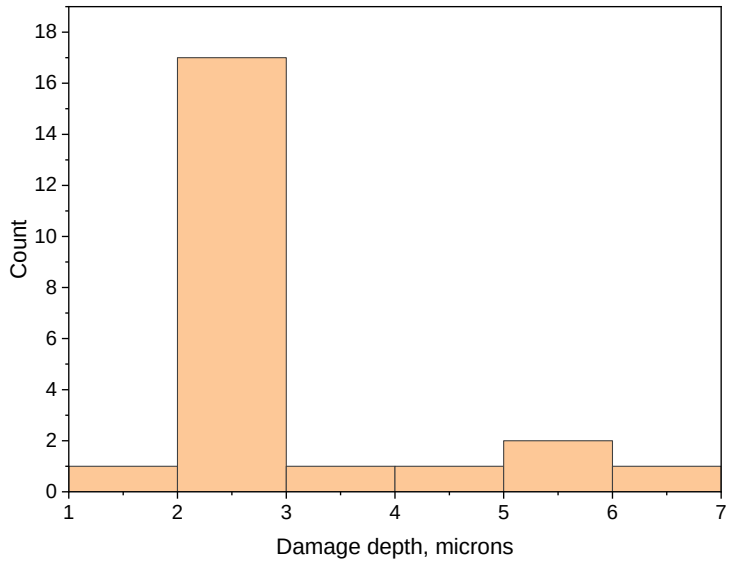

Figure 11. Number and depth of corrosion-related pits and cracks observed on the 4412-CS-1-1 specimen.

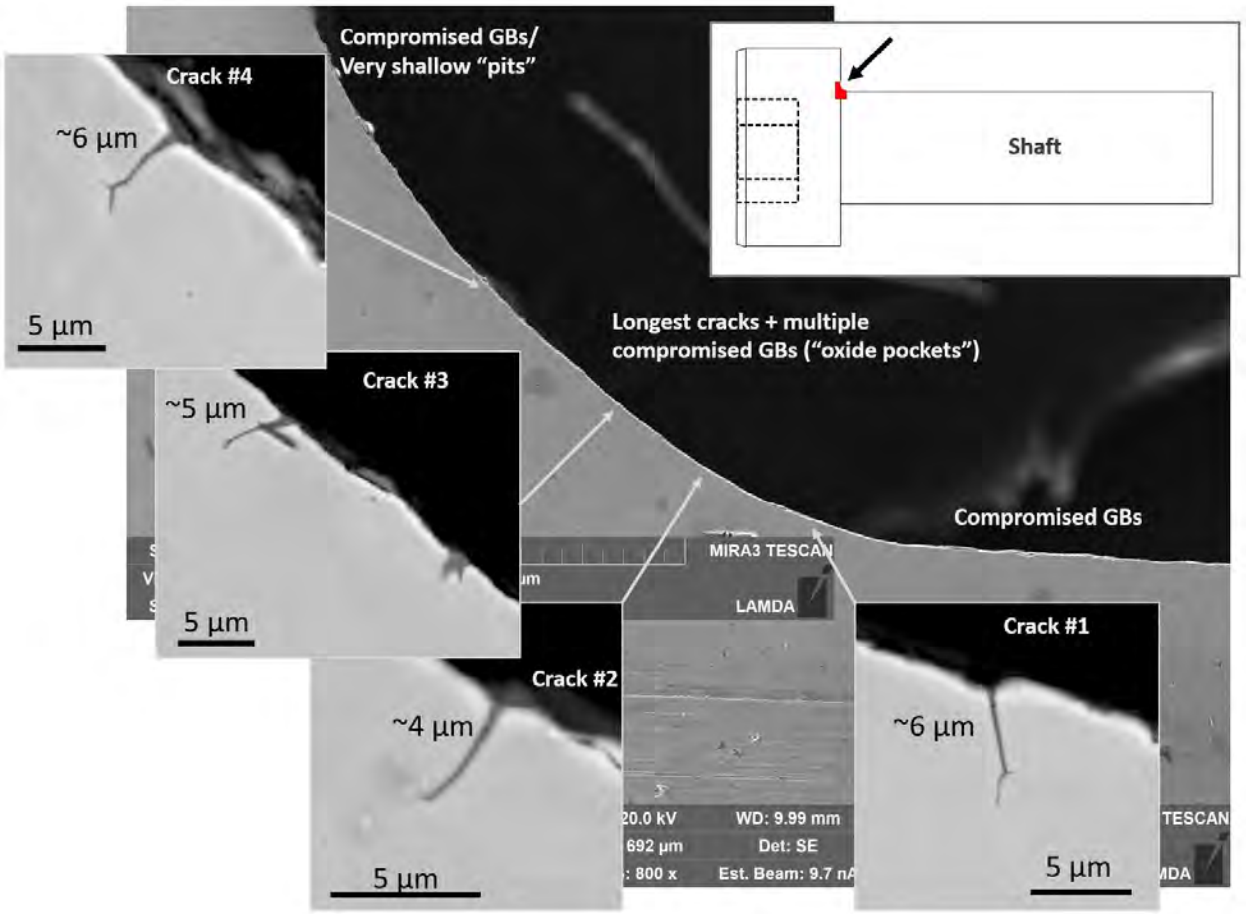

Figure 12. Identified cracks #1–#4 (objects with depths 4 µm+) located along the curved (circular) area of the BFB. Branching can be seen in cracks #1, #3, and #4. The collage combines low-magnification general view SE/SEM images with high-magnification BSE/SEM images taken for individual cracks. The inset at the top right shows the location and orientation of the area.

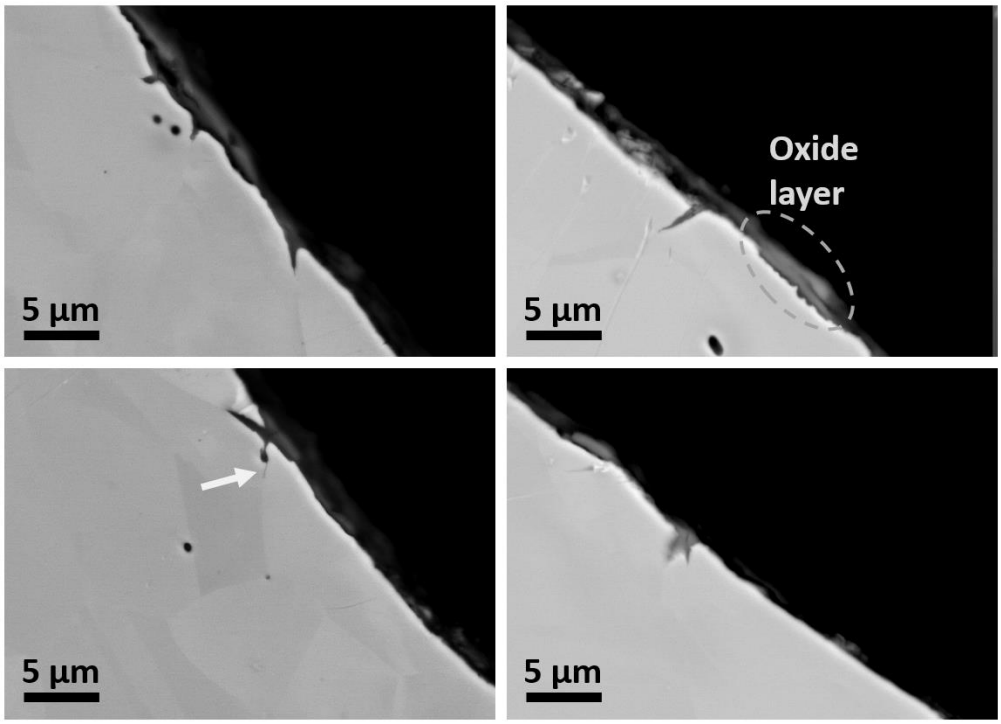

Figure 13. Enlarged view of degraded grain boundaries (SEM/BSE images). The damage penetrates at ~2–3 µm from the surface; features have triangle- or wedge-like shapes. Note the fine hair-like crack (indicated by white arrow) starting from the degraded boundary in the bottom left image. A dashed oval shows a remnant of the oxide layer.

3.3 EDS ANALYSIS OF THE CRACKS

Figure 14 and Figure 15 show the results of SEM/EDS scans performed for the identified cracks. The figures show that the cracks are filled with Cr- and O-rich substances, most likely Cr-rich oxide. Mo enrichment exists in the near-surface layer and near the crack "mouth." There is also some depletion in Ni and minor enrichment in Mn inside the cracks. Mn enrichment should be confirmed because EDS tends to overestimate Mn in austenitic steel irradiated in power reactors with thermal spectra.

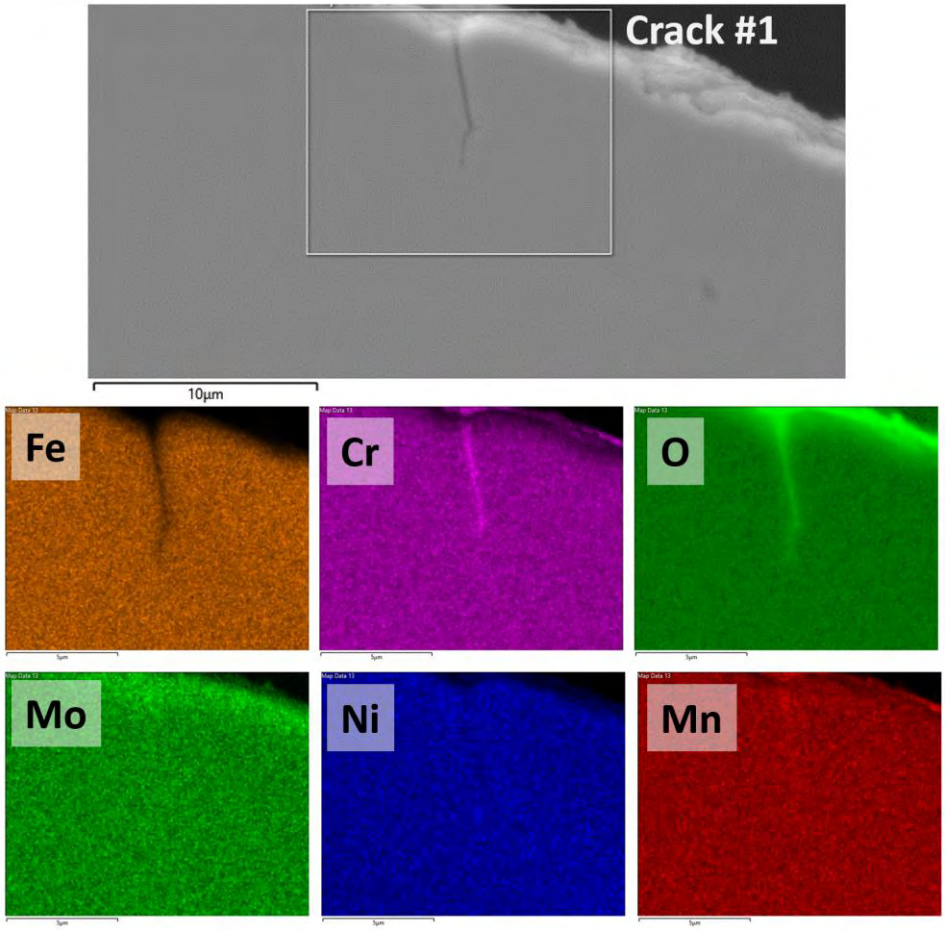

Figure 14. SEM/EDS maps for Crack #1 shown in Figure 12. The crack is likely filled with Cr-rich oxide. Oxygen enrichment along the surface suggests the presence of an oxide layer.

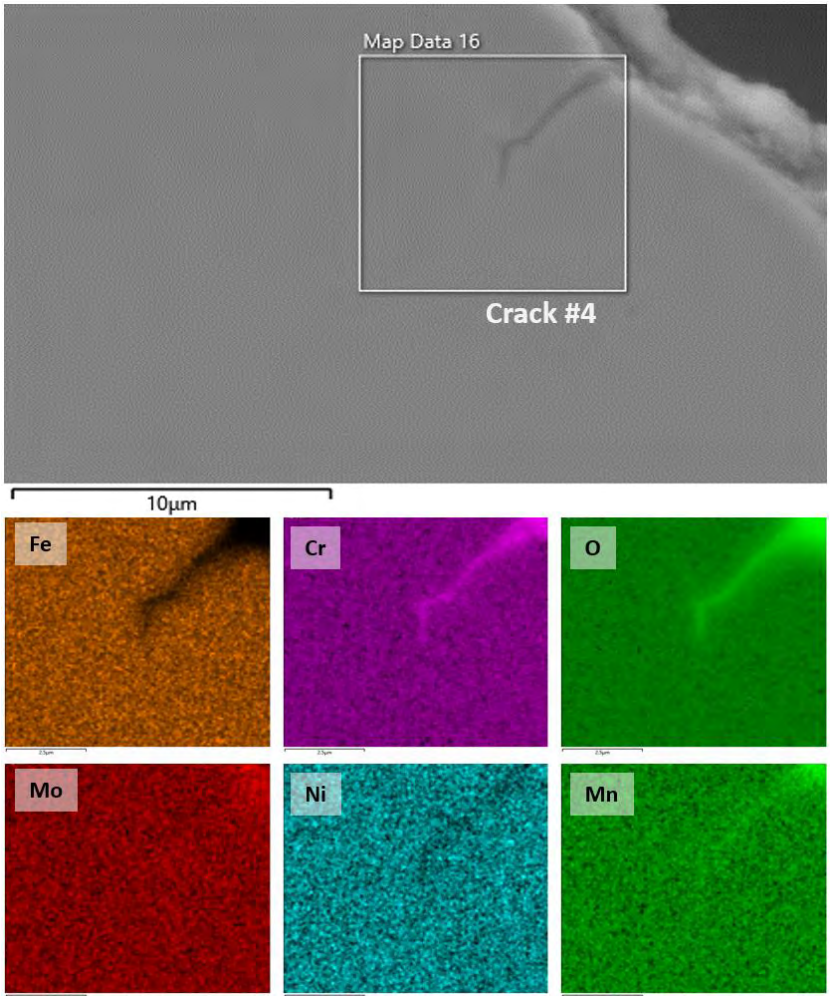

Figure 15. SEM/EDS maps for Crack #4 shown in Figure 12.
The SEM image suggests the presence of a surface oxide layer.

3.4 INTERGRANULAR NATURE OF THE DAMAGE

Figure 16 shows the grain's microstructure and the character of grain boundaries (misorientation in degrees and random type high-angle boundary [RHAB] or Σ3) in the vicinity of Crack #4. The crack propagated in an intergranular fashion can be seen along grain boundaries. At triple junction points, the crack tended to branch, and new branches also formed along the GBs. Only RHABs were involved in cracking. Although there was a short Σ3-boundary, the crack moved along the RHAB after reaching the triple junction point, and Σ3 was immune.

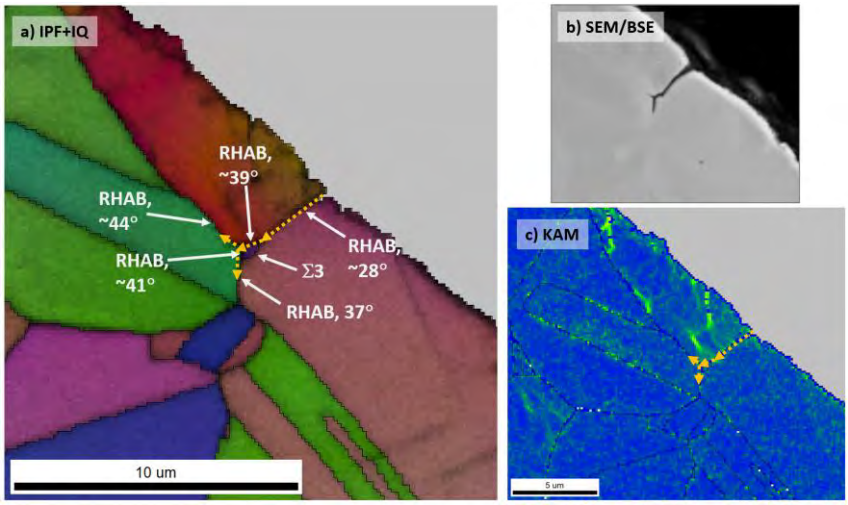

Figure 16. Grain microstructure in the vicinity of Crack #4 (Figure 12): (a) IPF+IQ, (b) SEM/BSE image, and (c) KAM map for the same location. The crack propagated in an intergranular fashion and along RHABs.

3.5 RELATIONSHIP BETWEEN CRACKS AND OXIDE LAYER AT THE SPECIMEN SURFACE

A survey of the BFB surface exposed to high-temperature high-pressure water (Figure 17) revealed a thin crack in the oxide layer. The crack in the oxide layer appears to be connected with Crack #3, as observed at the BFB cross-section.

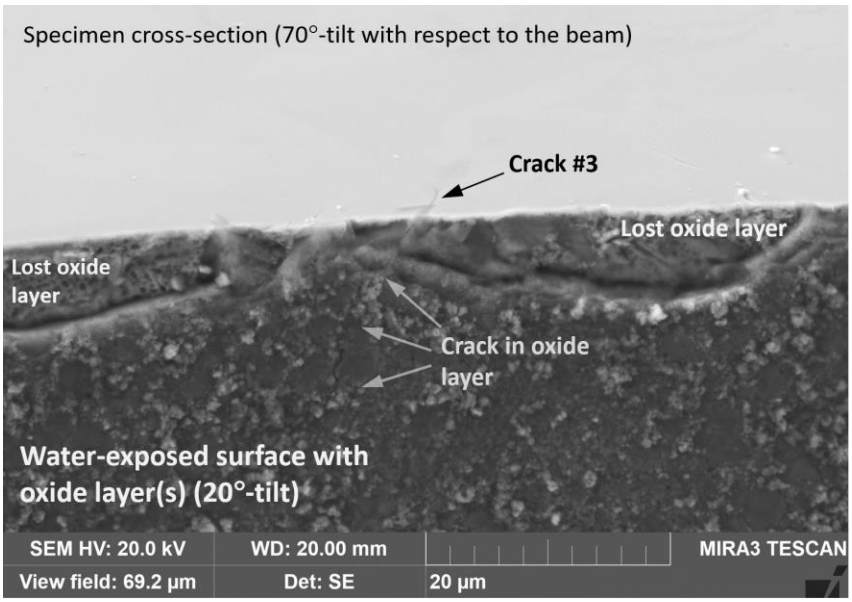

Figure 17. Crack in the oxide layer in the vicinity of Crack #3. Note that the oxide layer was lost directly near the specimen edge (likely during specimen preparation). The water-exposed surface shows partially preserved oxide particles, (some of which were likely removed during component handling).

Figure 18 provides additional evidence regarding spatial correlation of corrosion cracking in the BFB, as well as cracking (likely of mechanical origin) in the oxide layer.

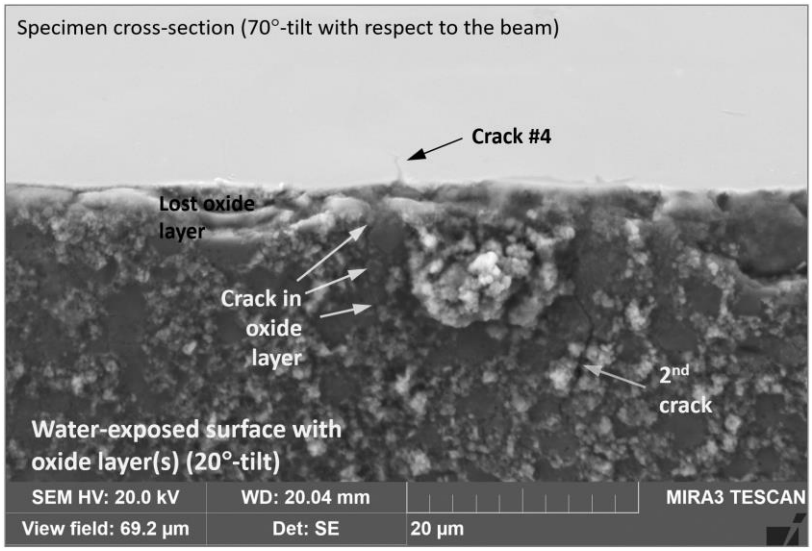

Figure 18. Oxide layer cracking in the vicinity of Crack #4. A second crack can also be observed, likely correlating with the degraded grain boundary.

4. MICROSTRUCTURE TO REVEAL THE COMPLEX HISTORY OF COMPONENT AND IN-SERVICE DEGRADATION

Observation of abnormal grains and variations in their numbers, as well as the appearance of a near-surface deformed layer, suggest an important possibility that instead of being perceived as deleterious, microstructure defects can act as an important source of information about processes that occurred during component fabrication and in service [9]. EBSD may sufficiently survey large areas at different magnification levels, thus providing macro- and meso-scale information. If a proper interpretation is possible, then the defect microstructure may act as a *material-state fossil record* (the term is offered in [9]) representing a component's in-service conditions.

To assess this concept, a larger region around Crack #4 was scanned using EBSD, as shown in Figure 19. Based on an analysis of the EBSD maps, multiple signs of plastic deformation can be recognized, some relating to specimen preparation (i.e., scratches formed during preparation). The scratches may start and end inside the grain (see a group of scratches in area S_m and individual examples S_1 through S_3). Scratches intersect grain boundaries without changing directions. Also, the scratches do not follow (111)-plane traces (usual slip traces for fcc-materials) except in rare coincidental cases. Scratches often form in groups and appear as parallel lines.

If the scratches are excluded, then the remaining plastic deformation signs will be pre-service (pre-irradiation, including manufacturing) strain-induced, and in-service or post-irradiation features. Pre-service damage may be seen in grains G_1, G_2, and G3, which are likely the result of AGG, as described in Section 3.1. Furthermore, minor in-grain misorientation exists in the near-surface layer. The AGG-related features and plastic strains in the near-surface layer are of limited interest here and should be excluded.

Because the remaining features are of very high importance in this effort, F_1—a dark line starting and ending at grain boundaries—exists within one grain and follows the (111)-plane trace (see Figure 20) with reasonable accuracy. Following the (111)-plane trace is a very strong sign of a strain-induced feature, a slip line or a defect-free channel; however, the accuracy (angular difference between predicted and projected plane traces) of this sign is limited by the EBSD system absolute error, which is usually less than a degree, and it might be larger near the specimen edges because the specimen edges are not

completely flat and often have rounded shape caused by preparation (mechanical polishing). The F_1 feature appearance in the IQ map closely resembles the defect-free channel typically observed in irradiated and deformed austenitic steels [8]. The F_2 group also belongs to one grain and agrees well with expected slip plane traces, as do F_3 and F_4.

It is possible to conclude that objects F_1 through F_4 are defect-free channels formed at some point after the material reached ~2–5 dpa. The appearance of defect-free channels strongly suggests that the material reached levels of stress that were close to yield stress (YS). The exact stress level and loading conditions are unknown; channels may form at stress levels as low as ~0.8 YS in a routine tensile test and at ~0.5 YS during slow strain rate testing. Because channels exist only in some grains and the majority of grain population is channel free (i.e., no bulk deformation is observed, by analogy with [10]), slow loading may be expected at stresses comparable but still below the bulk YS.

Although the exact stress level is under question, channel existence undoubtedly points out the presence, at least episodical, of high stresses disturbing the component's microstructure.

In this work, it is important to underline one critical aspect regarding defect-free channel formation during service. Figure 20, which shows features F_1–F_4 in more detail, illustrates strong differences in the channel contrast under the same scanning conditions (compare F_1 and F_2, F_3, and F_4 in the IQ map). This suggests the possibility that the channels formed at different times during service. It is not clear how a newly formed channel behaves under continuous irradiation. When a channel forms, the existing radiation-induced defects disappear, being swept away by moving dislocations. However, if radiation continues, then the channel would be filled with newly formed defects and would become weakly recognizable or even invisible.

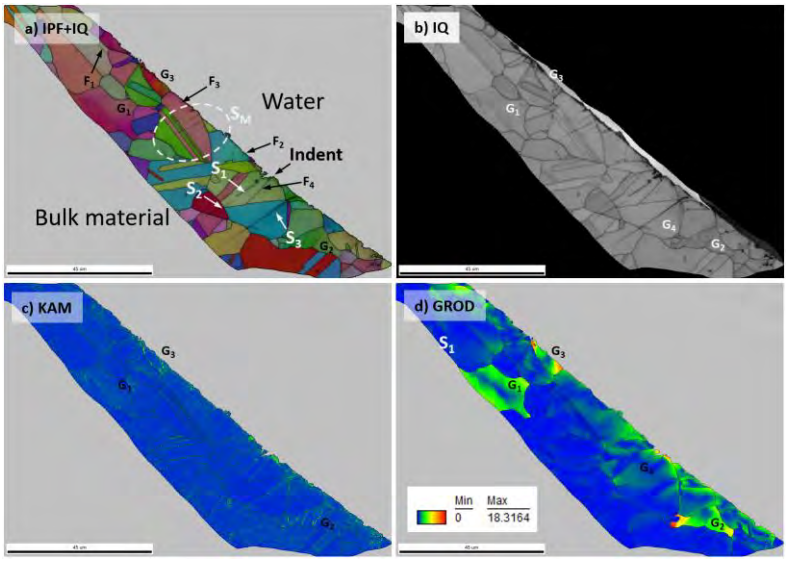

Figure 19. EBSD dataset for the area surrounding Crack #4. Multiple signs of plastic deformation can be seen in many grains. S_M indicates the area with multiple short scratches; S_1, S_2, and S_3 indicate believed-to-be scratches; and F_1 through F_4 show strain-induced features.

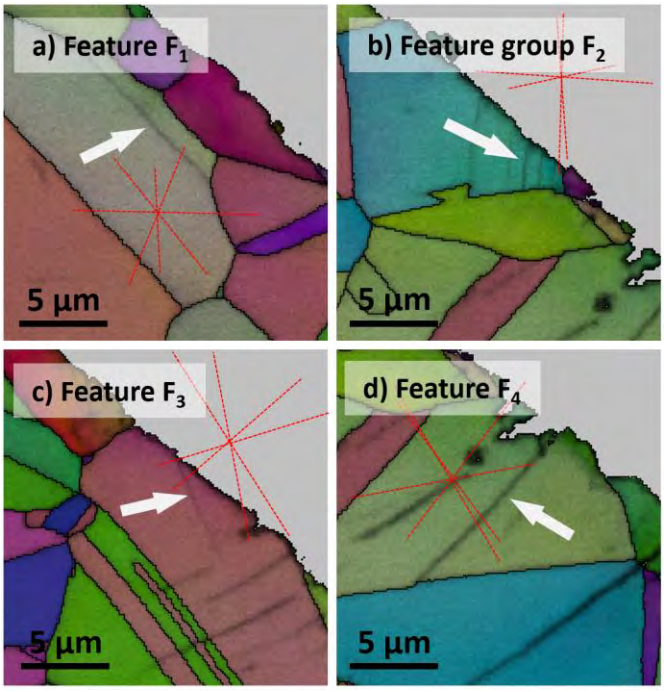

Figure 20. Detailed view of the features F_1 through F_4 from Figure 19. Red dashed lines show projections of (111)-slip planes (possible slip traces). Good agreement in orientation **can be observed** between a slip plane projection and features F_1 and F_2, reasonable agreement for F_3, and a deviation of about 5° for F_4.

This possibility of meso-level microstructural analysis and its interpretation to reveal a component's history should be explored further.

5. SUMMARY AND CONCLUSIONS

This report documents the results of the microstructure evaluation of the baffle-former bolt, a commercial PWR component. SEM/EDS analysis confirmed the material to be AISI 316 steel, having an annealed austenite microstructure with a limited fraction of grains undergoing abnormal grain growth. No retained ferrite was observed.

Evaluation of the specimen areas that had been exposed to high-temperature, high-pressure water during service showed clear signs of corrosion degradation, which likely occurred in service. EBSD analysis identified the corrosion as intergranular. The degraded areas may be categorized into two types, the first being *grain boundary degradation* that is most likely caused by grain boundary oxidation. The depths of these areas are less than 3 µm. The second type – *cracking* – is characterized by short cracks with depths of approximately 5–6 µm. EDS analysis detected the presence of Cr-rich oxides within these cracks. The current data set is limited and does not conclusively confirm or refute the existence of longer cracks. An experiment involving oxide layer removal may be beneficial for studying GB degradation; in this case, if oxide layer is chemically removed, GB degradation may be studied with better statistics.

Detailed EBSD data analysis indicates the presence of defect-free channels and evidence of plastic deformation. The defect-free channel formation is an active deformation mechanism. Its presence suggests that the analyzed BFB experienced episodic high mechanical stresses comparable to yield stress while in service. Analysis of EBSD data with respect to the active deformation mechanism and localized strain indicated in-service damage. A thorough analysis of in-service damage may allow for retrieving component history.

At this juncture, there is confidence that the available specimens offer a critically important and potentially unique opportunity to study the in-service–induced degradation of NPP components. Although the corrosion layer is intricate, it remains undisturbed, and the underlying layer reflects the in-service history of the component. Data analysis is ongoing, and further research is planned to provide a more comprehensive statistical overview and detailed insights.

REFERENCES

[1] K.J. Leonard, M.A. Sokolov, M.N. Gussev, Post-Service Examination of PWR Baffle Bolts, Part I. Examination and Test Plan, Oak Ridge National Laboratory Report, ORNL/LTR-2015/193, 2015.

[2] X.F. Chen, M.A. Sokolov, Fracture Toughness and Fatigue Crack Growth Rate Testing of Baffle-Former Bolts Harvested from a Westinghouse Two-Loop Downflow Type PWR, Oak Ridge National Lab.(ORNL), Oak Ridge, TN (United States), 2021.

[3] T. Lach, X. Chen, T.M. Rosseel, Microstructural Characterization of the Second High Fluence Baffle-Former Bolt Retrieved from a Westinghouse Two-loop Downflow Type PWR, Oak Ridge National Lab.(ORNL), Oak Ridge, TN (United States), 2022.

[4] X.F. Chen, T. Chen, C.M. Parish, T. Graening, M.A. Sokolov, K.J. Leonard, Post-Irradiation Examination of High Fluence Baffle-Former Bolts Retrieved from a Westinghouse Two-Loop Downflow Type PWR, Oak Ridge National Lab.(ORNL), Oak Ridge, TN (United States), 2019.

[5] M. Gussev, Dixon, Travis, Chen, Xiang, Analysis of Deformation and Fracture Mechanisms in the Harvested Low-Dose Baffle Former Bolt via Advanced Mechanical Tests, Oak Ridge National Lab.(ORNL), Oak Ridge, TN (United States), 2023.

[6] O.K. Chopra, A.S. Rao, Degradation of LWR Core Internal Materials due to Neutron Irradiation, 2010.

[7] F. Najafkhani, S. Kheiri, B. Pourbahari, H. Mirzadeh, Recent advances in the kinetics of normal/abnormal grain growth: A review, Archives of Civil and Mechanical Engineering. 21 (2021) 1–20.

[8] M.N. Gussev, K.J. Leonard, In situ SEM-EBSD analysis of plastic deformation mechanisms in neutron-irradiated austenitic steel, Journal of Nuclear Materials. 517 (2019) 45–56.

[9] K. O'Donnell, M.J. Quintana, M.J. Kenney, P.C. Collins, Using defects as a 'fossil record' to help interpret complex processes during additive manufacturing: as applied to raster-scanned electron beam powder bed additively manufactured Ti–6Al–4V, Journal of Materials Science. (2023) 1–24.

[10] K.J. Stephenson, G.S. Was, The role of dislocation channeling in IASCC initiation of neutron irradiated stainless steel, Journal of Nuclear Materials. 481 (2016) 214–225.